Distributed Validation and Testing of EV Systems

- Results of the European Project XILforEV -

Valentin Ivanov [1], Viktar Beliautsou [1], Florian Büchner [1]

1) Automotive Engineering Group, Technische Universität Ilmenau, Ilmenau, Germany

E-mail: valentin.ivanov@tu-ilmenau.de

ABSTRACT: The presented study addresses the methodology for building distributed test platforms that support the design of electric vehicle (EV) systems and the validation of their functionality. The platforms are implemented in the form of an X-in-the-loop (XIL) architecture and may include multiple test setups united in a local or geographically remote network. The communication of the networked test setups is based on the User Datagram Protocol (UDP). The paper presents the realization of the XIL environment suitable for the development of EV control systems such as brake blending, ride blending (RB) and integrated chassis control (ICC). For this purpose, the dynamometric test setup for the in-wheel motor, the hardware-in-the-loop (HIL) brake test bench, the shaker for the suspension actuators, and the driving simulator are integrated into the XIL environment. The results show the validation of the controllers for several complex maneuvers.

KEY WORDS: x-in-the-loop, electric vehicle, testing, in-wheel motor, brake-by-wire, active suspension

1. INTRODUCTION

The increasing complexity of vehicles is leading to new approaches to validation and testing at the component and system level. This is particularly relevant for electric vehicles, where different domains (e.g., E/E, mechanical and mechatronic systems) should be considered during testing. Some technologies in this regard are based on the coupling and networking of multiple test devices, accompanied by appropriate simulation tools, which are discussed in recently published studies. [(1)-(4)] In the present study, a variant of networked test platforms is also considered. This variant [(5)] allows the geographically distant test devices to communicate via the Internet. One of the advantages of the proposed approach is the possibility of complex real-time (RT) experiments, which require simultaneous analysis of cross-domain processes on different test devices.

The paper also presents the architecture of the developed test environment, use cases illustrating its operation, and analysis of the obtained results.

2. XIL ARCHITECTURE

As shown in Fig. 1, the proposed XIL architecture has a multi-layer topology and a "master-slave" organization. A test facility can be selected as the "master", which coordinates the operation of other facilities ("slaves") with installed EV systems and in which the whole RT vehicle model is executed. An EV system can be implemented as a RT software (SW) or hardware (HW) application. Considering that the involved test facilities may operate with different internal control software, a layer can be added for co-simulation purposes, e.g. based on the functional mockup interface (FMI). In the present study, the communication between the test facilities was organized over local area networks or the Internet and uses the UDP protocol. To minimize jitter and data loss, the test systems are connected to the same Virtual Private Network (VPN). Each VPN site has a static IP address to minimize the time delay in communication.

The XIL architecture described was implemented to connect multiple test platforms in different geographic locations, as shown in Fig. 2. The "master" component is the advanced driving simulator in Delft (The Netherlands) with the RT full vehicle model, created in Simcenter Amesim software. Emulation of the vehicle's traction and braking dynamics was organized using the HIL brake system test rig and the In-Wheel Motor (IWM) test rig. Both platforms are operated in Ilmenau (Germany). For ride quality control, the test bench with the active suspension actuator was included. This platform is located in Zaragoza (Spain).

The time delays during the experiments between the test hosts, measured as round-trip time during data exchange, were in the range of 16...45 ms, which allows testing the control functions with the RT capability for most EV applications.

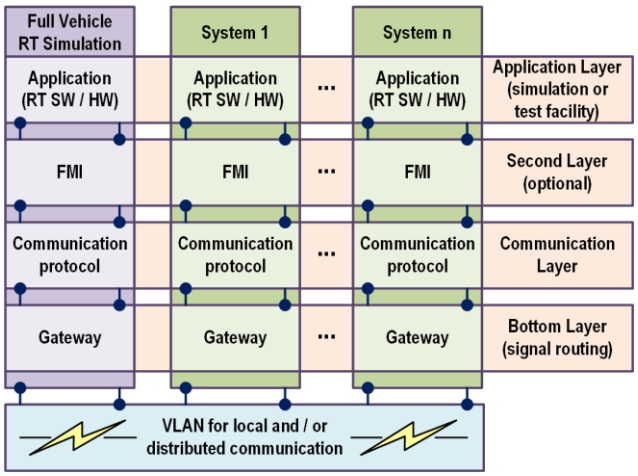

Fig. 1 XIL Architecture.

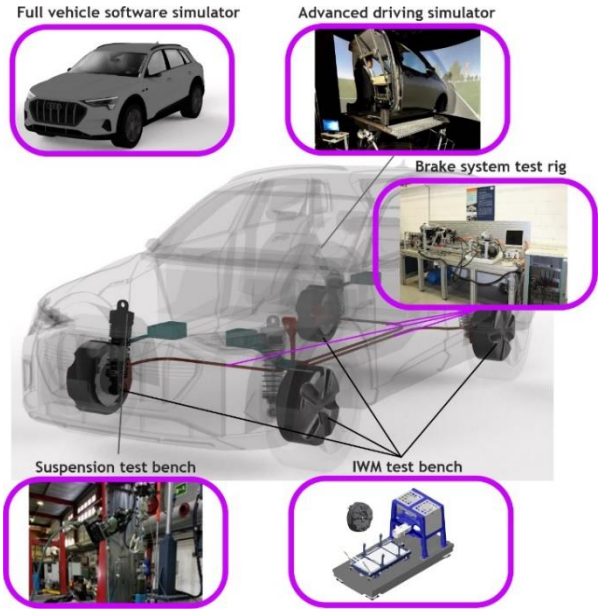

Fig. 2 Realization of XIL Architecture with Different Test Setups.

From an XIL communication perspective, it is important to note that the time delays could critically affect the overall performance of the test procedures. However, with the proposed technology based on VPN and UDP components, reasonable delays could be achieved, as shown in Fig. 3. Thus, the requirements for RT operation were met for the vehicle motion control studies during critical maneuvers. Some other configurations of the XIL environment were also created to study braking operations and fail-safety control. (6) However, these variants are not the subject of the present work. Several use cases were investigated using the test environment shown in Fig. 2. In this paper, relevant results are presented for the use cases that validate the functionality of ride blending and integrated chassis control.

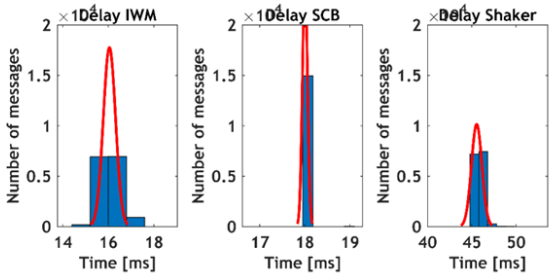

Fig. 3 Communication Delays by Networking IWM test Bench (*left*), Brake System Test Rig (*middle*) and Suspension Test Bench (*right*) as Applied to ICC Test

3. USE CASES

3.1. EV configuration

The experiments were conducted for a sport utility vehicle with the data given in Table 1. The RT full vehicle dynamics model was developed in Simcenter Amesim and run on the driving simulator. The devices under test of the in-wheel motor, the decoupled braking system with friction brakes, and the actuator for the active suspension were installed on the corresponding test platforms as shown in Fig. 2. Thus, the entire EV corner with drivetrain and chassis elements were included as real hardware components. The operation of the other three corners of the vehicle was modeled using the hardware corner as a reference and applying different scaling factors required to account for different loading modes between the front and rear axles and between the left and right wheels during the maneuvers.

Table 1 EV Data.

Vehicle parameter	Value
Gross weight	2578 kg
Max. velocity	181 km/h
Type of drivetrain	4WD, in-wheel motors
Electric motor	
Max. torque (300 rpm)	1500 Nm (> 10 sec)
Cont. torque (800 rpm)	800 Nm
Max. output power	110 kW (1500 Nm, 700 rpm)
Cont. output power	65 kW (650 Nm, 955 rpm)
Active suspension	
Force range	-6000 N ... 5000 N
Decoupled brake system	
Type	electro-hydraulic
Max. brake pressure	160 bar

3.2. Controller structure

Figure 4 shows the structure of the controller that combines both the RB and the ICC. The difference is mainly in the actuators involved. Ride blending is a technology for electric vehicles that aims to control ride quality through both IWM and active suspension. It is based on the effect that the vertical force can be generated by an IWM based on the fluctuations of the instantaneous center of the front and rear suspensions, Fig. 5. Therefore, the joint operation of IWM and suspension actuators can be used to control the heave, roll, and pitch dynamics of EV. Some papers provide further information on IWM control of vertical motion [7]-[9] and on the RB approach. [10]

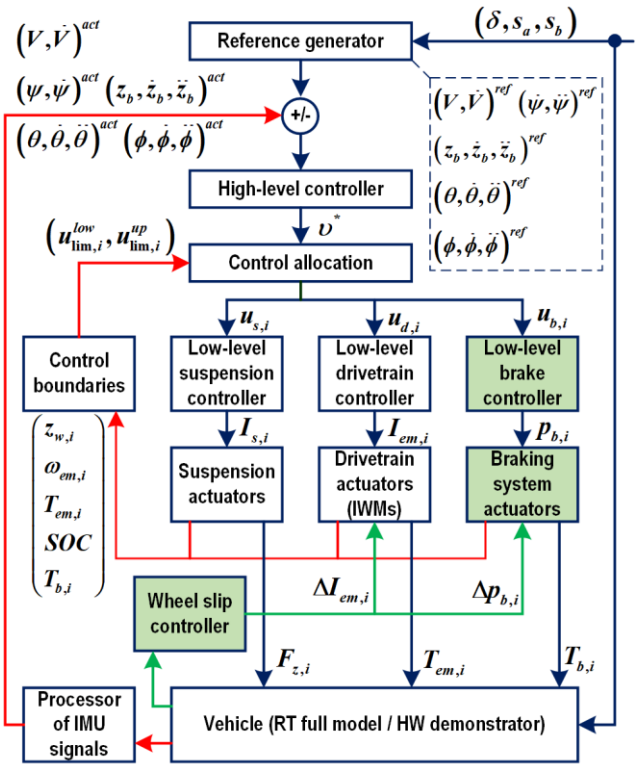

Fig. 4 Structure of Ride Blending and Integrated Chassis Controller.

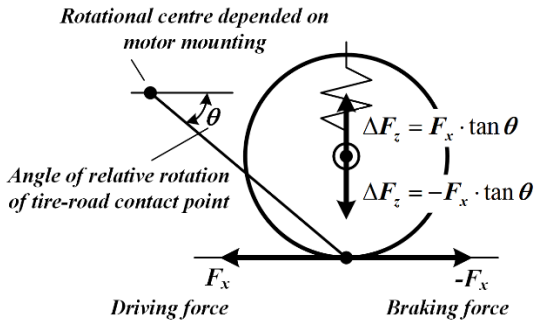

Fig. 5 Principle of Changing the Vertical Tire Force Through by Mounting the Electric Motor (reproduced from [11]).

While only the active suspension and the drivetrain are involved in the RB, the ICC additionally includes the braking system (*in this context, the control blocks that are only relevant for the ICC are colored green in Fig. 4*). At the level of control logic, the difference is that the RB aims at improving ride quality, while the ICC aims at optimizing driving safety and comfort as well as energy efficiency at the same time. The control process can be briefly outlined as follows.

The reference generator defines a set of the following reference states for the vehicle body motion: vehicle velocity and acceleration $(\boldsymbol{V}, \dot{\boldsymbol{V}})^{\boldsymbol{ref}}$; yaw angle and rate $(\boldsymbol{\psi}, \dot{\boldsymbol{\psi}})^{\boldsymbol{ref}}$; vertical displacement, vertical rate, and vertical acceleration $(\boldsymbol{z_b}, \dot{\boldsymbol{z}}_{\boldsymbol{b}}, \ddot{\boldsymbol{z}}_{\boldsymbol{b}})^{\boldsymbol{ref}}$; pitch angle, pitch rate, and pitch acceleration $(\boldsymbol{\theta}, \dot{\boldsymbol{\theta}}, \ddot{\boldsymbol{\theta}})^{\boldsymbol{ref}}$; roll angle, roll rate, and roll acceleration $(\boldsymbol{\phi}, \dot{\boldsymbol{\phi}}, \ddot{\boldsymbol{\phi}})^{\boldsymbol{ref}}$. Depending on the goals of the RB or ICC control (e.g., driving safety, driving comfort, road holding, handling, and others), either the entire parameter set or only a few selected parameters are used as the control reference. The vehicle motion reference state is obtained from a reference vehicle model. To detect the maneuver conditions, the reference generator unit uses as input parameter the accelerator pedal travel $\boldsymbol{s_a}$, the brake pedal travel $\boldsymbol{s_b}$, and the steering wheel angle $\boldsymbol{\delta}$. The deviations of the generated reference states from their actual values (marked ***"act"*** in Fig. 4) are used as inputs to the high-level controller.

The high-level controller generates the virtual control input $\boldsymbol{v}^*$ for the control allocation unit. The virtual control input $\boldsymbol{v}^*$ consists of several components: $\boldsymbol{v}^* = [\boldsymbol{\Delta F_x}\ \boldsymbol{\Delta M_\psi}\ \boldsymbol{\Delta F_z}\ \boldsymbol{\Delta M_\theta}\ \boldsymbol{\Delta M_\phi}]$, $\boldsymbol{\Delta F_x}$ is the longitudinal force, $\boldsymbol{\Delta M_\psi}$ is the yaw moment, $\Delta \boldsymbol{F_z}$ is the vertical force, $\Delta \boldsymbol{M_\theta}$ is the pitch moment, and $\Delta \boldsymbol{M_\phi}$ is the roll moment required to offset the error between the considered reference and actual states.

The control allocation unit uses the virtual control input $\boldsymbol{v}^*$ to derive the control demands $\boldsymbol{u_{b,i}}$ for the low-level braking system controller, $\boldsymbol{u_{d,i}}$ for the low-level drivetrain controller and $\boldsymbol{u_{s,i}}$ for the low-level suspension controller. The control allocation problem is formulated as minimizing the allocation error and control actuations, taking into account optimization constraints, as proposed in previous work. [12]

The control allocation unit also takes into account the lower $\boldsymbol{u_{lim,i}^{low}}$ and upper $\boldsymbol{u_{lim,i}^{up}}$ actuator *constraints* that limit the possible forces of the suspension and braking system as well as the IWM torques. The constraints on the actuators with respect to the suspension are calculated from the positions $\boldsymbol{z_{w,i}}$ of the suspension

actuators. The constraints for the actuators of the drivetrain system are calculated from the speed $\boldsymbol{\omega_{em,i}}$ and torque $\boldsymbol{T_{em,i}}$ of the electric motors, as well as from the state of charge ***SOC*** of the battery. The constraints for the braking system are calculated from the wheel braking torques $\boldsymbol{T_{b,i}}$ of the braking system.

The low-level suspension controller calculates the control current $\boldsymbol{I_{s,i}}$ for each suspension actuator to generate the required vertical forces $\boldsymbol{F_{s,i}}$. The low-level drivetrain controller calculates the control current $\boldsymbol{I_{em,i}}$ for each IWM actuator to generate the required braking torques $\boldsymbol{T_{em,i}}$. The low-level braking system controller calculates the brake pressure $\boldsymbol{p_{b,i}}$ for each caliper to produce the required brake torques $\boldsymbol{T_{b,i}}$. In addition for the ICC, in case the torque applied to the wheel causes it to slip beyond a certain threshold, *the wheel slip controller* reduces the torques to be generated by the electric motor or the friction brake.

3.3. Evaluation of XIL accuracy

Due to the complexity of the XIL architecture and use cases, it is necessary to verify that the distributed test procedures can guarantee sufficient precision of the experiments. To this end, XIL performance was evaluated by comparing the same maneuvers in the high-fidelity simulation environment with multi-body vehicle model and in the XIL environment, using the normalized root mean square error *NRMSE* between maximum and minimum values of the simulated and XIL-tested results as the main indicator:

$$NRMSE = \frac{\sqrt{\frac{1}{n}\sum_{i=1}^{n}\left(x_{i,simulated} - x_{i,XIL}\right)^2}}{Data_{\max} - Data_{\min}}. \quad (1)$$

For purely longitudinal maneuvers such as the straight-line braking, the accuracy can be illustrated using Fig. 6 and Table 2. It can be confirmed that the distributed XIL architecture for modeling vehicle dynamics is very accurate for the proposed maneuver. The highest error, exceeding 10% NRMSE, is found for the parameters affecting the lateral dynamics. This error value could be explained by the inaccuracy of the simulation caused by replacing the vehicle suspension model with the real model. Nevertheless, the absolute error values are in a small range and cannot be perceived by a human in the driving simulator as a XIL component.

The performance of the XIL test environment for emulating lateral vehicle dynamics can be evaluated in Fig. 7 and Table 3 for the double lane change (DLC) maneuver. This is a more complex maneuver than straight-line braking. The accuracy of the simulation is assessed using the same criterion as for the braking maneuver. In this experiment, the highest NRMSE values are about 10% for vertical acceleration and pitch rate, which is acceptable for controller performance evaluation.

Therefore, it can be concluded that the developed XIL architecture can provide very good accuracy for the experiments with complex vehicle motion.

Table 2 Deviations Between the Results of Model Tests and XIL Experiments for Straight-line Braking Maneuver.

Vehicle parameter	NRMSE
Longitudinal acceleration	0.0189
Vertical acceleration	0.0623
Pitch rate	0.0352
Roll rate	0.1108

Table 3 Deviations Between the Results of Model Tests and XIL Experiments for Double Lane Change Maneuver.

Vehicle parameter	NRMSE
Longitudinal acceleration	0.0429
Lateral acceleration	0.0460
Vertical acceleration	0.1377
Pitch rate	0.1344
Roll rate	0.0504
Yaw rate	0.0271

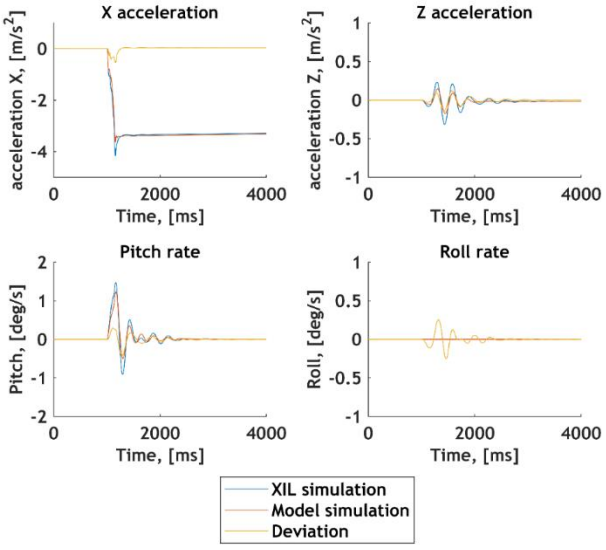

Fig. 6 Comparison of XIL Experiments and RT Model Tests for the Straight-line Braking Maneuver.

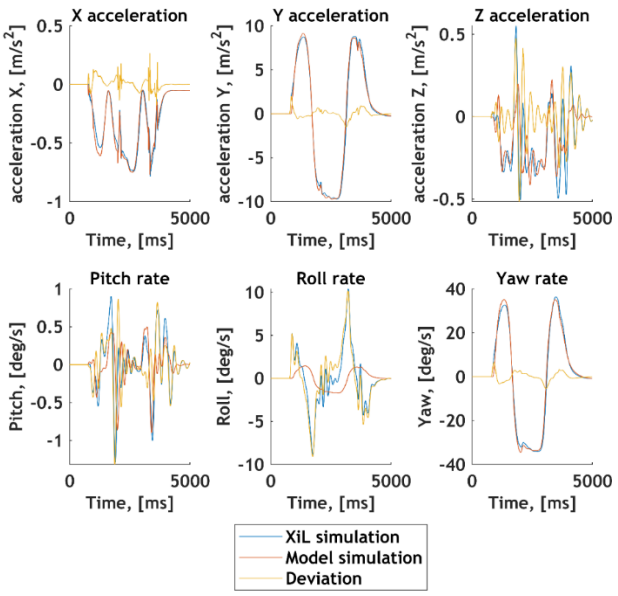

Fig. 7 Comparison of XIL Experiments and RT Model Tests for the Double Lane Change Maneuver.

3.4. Test results

RB and ICC operations were evaluated in three maneuvers – straight-line braking, double lane change, and braking in a turn – using Key Performance Indicators (KPI) for safety and comfort. The KPI for safety corresponds to the RMSE value of the wheel load fluctuations (road holding) and is calculated as:

$$RMSE = \frac{1}{4}\sum_{r=1}^{m,j}\sqrt{\frac{1}{n}\sum_{k=1}^{n}\left(F_{wheel,i} - F_{static,i}\right)^2}\,, \quad (2)$$

where $F_{wheel,i}$ is the vertical load on a tire during an experiment, $F_{static,i}$ is the vertical load on that tire for a standing vehicle, the indices *m* and *j* are for the front and rear wheels respectively.

For comfort, the integrated criterion of ISO 2631 is proposed, which combines the weighted RMS value of vertical acceleration ($k = 1$), the weighted RMS value of pitch acceleration ($k = 0.4$), and the weighted RMS value of roll acceleration ($k = 0.63$).

To give an example of the experimental results obtained in the XIL test environment, Fig. 8 shows the comparison of different vehicle dynamic parameters for the DLC maneuver from 85 km/h for the reference vehicle without motion control and for the vehicle (so-called *passive mode*) with activated ICC. The general results of the functional evaluation of the RB and ICC systems are summarized in Table 4. In this table, the decrease in numerical indicators would correspond to an improvement in the vehicle motion quality of the maneuver.

Table 4 KPI for RB and ICC Evaluation*.

Maneuver	Setup	KPI Comfort	KPI Safety
Straight-line braking	Passive mode	3.4439	1.1989
	Ride Blending	**3.41591**	**1.1988**
Braking in a turn	Passive mode	**1.9954**	1.0395
	Ride Blending	2.6585	**1.0385**
Straight-line braking	Passive mode	1.2965	1.0431
	ICC	**0.9492**	**0.9676**
DLC at 85 km/h	Passive mode	64.7241	0.9833
	ICC	**17.8723**	**0.9959**
Braking in a turn	Passive mode	**4.3961**	1.0252
	ICC	4.4615	**1.0125**

* *Better values are marked in bold*

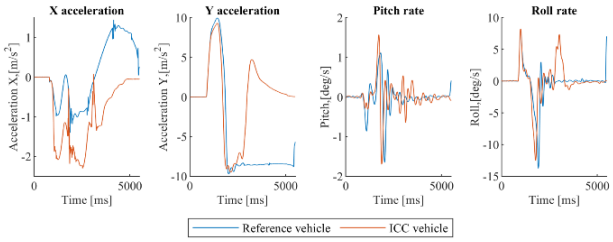

Fig. 8 Example of Experimental Results.

From the data obtained, it can be concluded for RB operation that a noticeable reduction in vertical force oscillations in the suspension can be observed for all maneuvers performed. For such critical maneuver as the braking in a turn, the RB redistributes control priorities so that driving safety is improved without critical degradation of ride quality.

It can be also concluded that the proposed ICC architecture is advantageous for EV dynamics by all criteria. In particular, ICC operation has improved safety during braking in a straight-line braking and braking in a turn. The improvement in comfort was essentially demonstrated for the critical double lane change maneuver at 85 km/h, where the reference vehicle cannot pass the required trajectory without ICC, and was also observed during the straight-line braking.

4. CONCLUSION

The distributed XIL test environment with the possibility of simultaneous RT operation of multiple test platforms and setups can be efficiently used for various validation and design tasks in the process of EV system development. Such an approach allows taking into account the real dynamics of actuators as well as complex loading processes that can hardly be simulated with conventional modeling tools. In the present work, these advantages have been demonstrated for use cases related to ride

blending and integrated chassis controller design. Another benefit of the distributed XIL environment is the overall reduction in testing and development time for new EV systems..

ACKNOWLEDGMENT

The project XILforEV leading to this application has received funding from the European Union's Horizon 2020 research and innovation programme under grant agreement No 824333. The authors would like to thank the colleagues from Audi (Germany), Elaphe (Slovenia), ITAINNOVA (Spain), Siemens Industry Software (Belgium and France), Tenneco Automotive (Belgium), EFS GmbH (Germany), Technische Universiteit Delft (The Netherlands), and Technische Universität Ilmenau (Germany) for their collaboration in this project.

REFERENCES

(1) P. Weber, S. Hähnlein, P. Rautenberg, and M. Gohl, "Potentials of Coupled Test Benches," *MTZ Worldwide*, vol. 83, pp. 66–70, 2022.

(2) M. Drechsler, V. Sharma, F. Reway, C. Schütz, and W. Huber, "Dynamic Vehicle-in-the-Loop: A Novel Method for Testing Automated Driving Functions," *SAE Int. J. of CAV*, vol. 5, no. 4, pp. 1-14, 2022.

(3) H. Bai, Q. Li, H. Luo, Y. Huangfu, and F. Gao, "Nonlinear Behavioral Modeling and Real-Time Simulation of Electric Propulsion System for the High-Fidelity X-in-the-Loop Applications," *IEEE Transactions on Transportation Electrification*, 2022.

(4) W. Niu, K. Song, Q. Xiao, M. Behrendt, A. Albers, and T. Zhang, "Transparency of a Geographically Distributed Test Platform for Fuel Cell Electric Vehicle Powertrain Systems Based on X-in-the-Loop Approach," *Energies*, vol. 11, no. 9, p. 2411, 2018.

(5) V. Schreiber, K. Augsburg, V. Ivanov, and H. Fujimoto, "Novel Developing Environment for Automated and Electrified Vehicles using Remote and Distributed X-in-the-Loop Technique," *IEEE Vehicle Power and Propulsion Conference (VPPC)*, Gijon, Spain, 2020.

(6) B. H. C. Sputh, L. Thielemans, J. Pašič, C. Ganier, and R. Pastorino, "Model-based real-time testing of fail-safe behavior for in-wheel motor propulsion systems," *IEEE Vehicle Power and Propulsion Conference (VPPC)*, Gijon, Spain, 2021.

(7) D. Akaho, M. Nakatsu, T. Katsuyama, K. Takakuwa, and K. Yoshizue, "Development of Vehicle Dynamics Control System for In-Wheel-Motor Vehicle," *JSAE Annual congress (Spring)*, Yokohama, Japan, 2010.

(8) T. Kobayashi, H. Sugiura, E. Katsuyama, A. Kawaguchi, and M. Hirano, "Energy Analysis of In-wheel Motor Vehicle with Active Ride Control," *R&D Review of Toyota CRDL*, vol. 46, no. 2, pp. 65-67, 2015.

(9) S. Murata, "Innovation by In-wheel-motor Drive Unit," *Vehicle System Dynamics*, vol. 50, no. 6, pp. 807-830, 2012.

(10) L. Hott, V. Ivanov, K. Augsburg, V. Ricciardi, M. Dhaens, M. Al Sakka, K. Praet, and J.V. Molina, "Ride Blending Control for AWD Electric Vehicle with In-Wheel Motors and Electromagnetic Suspension," *2020 IEEE Vehicle Power and Propulsion Conference (VPPC)*, Gijon, Spain, 2020.

(11) V. Ivanov, M. Dhaens, V. Ricciardi, D. Savitski, and K. Augsburg, "Ride Blending Control for Electric Vehicles," *The 31st International Electric Vehicles Symposium & Exhibition (EVS 31)*, Kobe, Japan, 2018.

(12) B. Shyrokau, D. Wang, D. Savitski, K. Hoepping, and V. Ivanov, "Vehicle motion control with subsystem prioritization," *Mechatronics*, vol. 30, pp. 297-315, 2015.